NANO LETTERS

2001
Vol. 1, No. 3
155−158

Magnetic Alignment of Fluorescent Nanowires

Monica Tanase,[†] Laura Ann Bauer,[‡] Anne Hultgren,[†] Daniel M. Silevitch,[†] Li Sun,[§] Daniel H. Reich,*[,†] Peter C. Searson,*[,§] and Gerald J. Meyer*[,‡]

Departments of Physics and Astronomy, Chemistry, and Materials Science and Engineering, Johns Hopkins University, 3400 North Charles Street, Baltimore, Maryland 21218

Received December 15, 2000

ABSTRACT

Nickel nanowires prepared by electrochemical growth in alumina templates have been removed from their templates and functionalized with luminescent porphyrins. The nanowires response to magnetic fields was quantified using video microscopy. In viscous solvents, magnetic fields can be used to orient the nanowires; in mobile solvents, the nanowires form chains in a head-to-tail configuration when a small magnetic field is applied. The dynamics for chain formation have been quantitatively modeled. The results demonstrate a new approach for assembling nanowires.

Colloidal solutions of spherical nanoparticles will spontaneously order into close-packed arrays under appropriate experimental conditions.[1−9] A great deal of research has been published on the self-assembly of spherical semiconductor and metal nanoparticles with interesting optical,[1−6] electronic,[7,8] and magnetic properties.[9] On the other hand, much less attention has been paid to the assembly and ordering of nanowires.[10−16] In principle, nanowires can be assembled into arrays and configurations not possible with spherical particles. We have recently initiated studies to assemble nanowires and elongated nanoparticles with the goal of creating ordered arrays with enhanced anisotropy. Here we report a magnetic approach for aligning and assembling fluorescent and nonfluorescent nanowires. Specifically, nickel nanowires functionalized with porphyrins and suspended in fluid solution can be oriented and assembled with magnetic fields. The assembly of nanowires into continuous chains has been quantitatively modeled by assuming that viscous drag and magnetic dipole−dipole interactions are the dominant forces. The results present a new approach for nanowire assembly.

Nickel nanowires were fabricated by electrochemical deposition into commercially available 50 μm thick alumina filter templates (Anodisc, Whatman, Inc.) with a nominal minimum pore diameter of 100 nm. A gold film was sputter-deposited on one side of the template to serve as a working electrode. Nickel was deposited from a solution of 20 g L^{-1} $NiCl_2 \cdot 6H_2O$, 515 g L^{-1} $Ni(H_2NSO_3)_2 \cdot 4H_2O$, and 20 g L^{-1} H_3BO_3, buffered to pH 3.4 at a potential of −1.0 V (Ag/AgCl).[17] The wires were grown to be 5−25 μm in length, as controlled by the deposition time. The nanowires' average radius was $a = 0.18 \pm 0.02$ μm, as determined by scanning electron microscopy. The wires are therefore nanometers in diameter and microns in length. The nanowires were removed from the templates by dissolving the alumina in 0.5 M KOH at $T = 50$ °C for 24 h, stirring occasionally. The wires were collected by centrifuging at 7000 rpm for 10 min, or by placing a small magnet on the side of the flask. This latter magnetic collection procedure exposed the wires to a field in excess of 1 kG and permanently magnetized the wires with their magnetic moments parallel to their long axis. With both procedures, the supernatant was decanted and the wires were resuspended by sonication in 1.5 mL of absolute ethanol. This collection and rinsing procedure was repeated twice with fresh ethanol or other solvents of interest and th esupernatant was generally stored in these solvents in air. Aggregation and settling of the wires was observed under a variety of conditions, and brief sonication (∼5 s, 42 kHz, Cole-Parmer model 8890) consistently resulted in redispersion of the wires, regardless of their remnant magnetization.

Nanowires suspended in low viscosity liquids such as water, ethanol, and 2-propanol precipitate from the solutions in the course of several minutes. In addition, aggregation occurs due to interwire magnetic forces. To minimize aggregation and precipitation, the nanowires were suspended in more viscous media such as 1:1 hexadecane ($C_{16}H_{34}$)/octadecane ($C_{18}H_{38}$) mixtures or ethylene glycol. These

[†] Department of Physics and Astronomy.
[‡] Department of Chemistry.
[§] Department of Materials Science and Engineering.

10.1021/nl005532s CCC: $20.00
Published on Web 03/14/2001

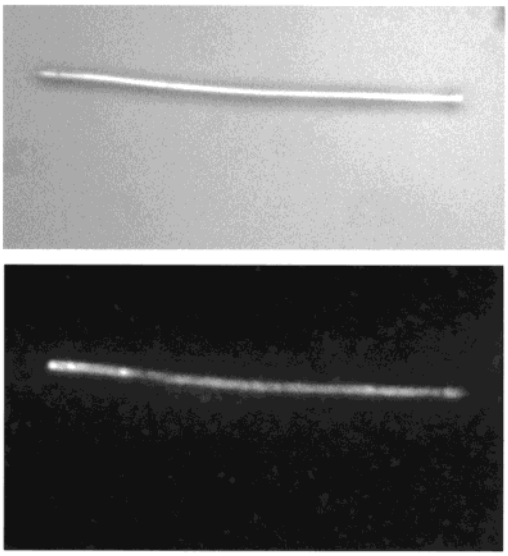

Figure 1. A 22 μm-long nickel nanowire, functionalized with Hematoporphyrin IX, and immobilized on a glass slide. The upper panel shows an optical image of the nanowire, while the lower panel shows a fluorescence image of the same wire.

suspensions are much more stable. For example, in hexadecane/octadecane the nanowires remained suspended for periods of days.

Porphyrins are an important class of macrocycles that regulate many biological processes such as the transport and activation of dioxygen.[18] Free-base porphyrins display intense fluorescence and are readily derivatized with functional groups that bind tenaciously to solid-state surfaces, but do not affect the fluorescent properties. To functionalize magnetic nanowires with fluorescent porphyrins, we chose Hematoporphyrin IX, [8,13-bis(1-hydroxyethyl)-3,7,12,17-tetramethyl-21*H*,23*H*-porphine-2,18-dipropionic acid], which has two intense, red fluorescence bands ($\lambda_{max} = 626$ and 696 nm in ethanol) and two carboxylic acid groups that are known to bind strongly to metal oxides and to the native oxide films on metals, such as nickel.[19] Reaction of the nanowires with mM concentrations of Hematoporphyrin IX for 24 h in ethanol at room temperature resulted in surface binding. The solution was then centrifuged, the supernatant decanted and saved, and fresh ethanol was added. This procedure was repeated until no fluorescence was observed from the supernatant solution. Typically between two and four iterations were required before the supernatant was nonemissive.

Figure 1a shows an optical microscope image, and Figure 1b shows the corresponding fluorescence image of a single, porphyrin-functionalized nickel nanowire deposited onto a glass slide by spin coating at 3000 rpm from an ethanol suspension. This spin-coating procedure yielded a large number of isolated wires, in contrast to evaporative deposition, which generally resulted in aggregation of the wires. The observation of fluorescence along the full length of the nanowires seen in Figure 1b suggests a uniform surface coverage. We note that porphyrin aggregation and energy transfer to metallic surfaces are known to quench molecular

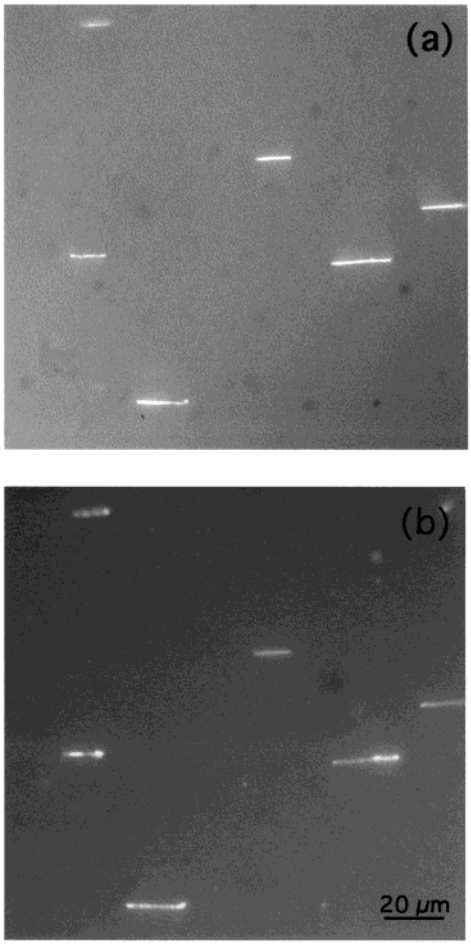

Figure 2. Assembly of 12 μm long nickel nanowires, functionalized with porphyrins and aligned in a magnetic field in a 1:1 hexadecane/octadecane mixture. The upper panel is an optical image, while the lower panel is a fluorescence image.

excited states.[20] One probable explanation for the intense steady-state fluorescence observed is that the emissive porphyrins are distant from the metallic nickel due to the native oxide film and the flexible ethane spacer between the carboxylic acid binding groups and the porphyrin ring. The porphyrin coatings on the nanowires were stable in ethanol for hours, although desorption does occur after a few days, as evidenced by fluorescence from the ethanol solutions. The nanowires remained fluorescent for weeks when stored in hexadecane/octadecane, water, or air.

The response of suspensions of nanowires to magnetic fields was investigated under optical and fluorescence microscopes. Even in the most viscous solvents, the nanowires respond to the torques produced by small uniform magnetic fields, and align parallel to the field, as shown in Figure 2. Magnetic field gradients, produced either by external magnets or by neighboring nanowires, exert forces on the nanowires, and provide means to manipulate and assemble them. For example, the 1000 G/cm field gradient produced by a small bar magnet, placed outside an experimental cell containing approximately 3 cm^3 of a water suspension, allows rapid collection of all the nanowires at the side of the cell in times of order 30 s.

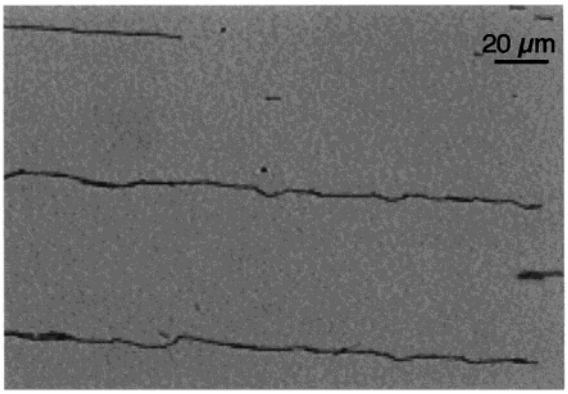

Figure 3. Chains of Ni nanowires, assembled from a water suspension on a glass substrate in a 20 G external magnetic field.

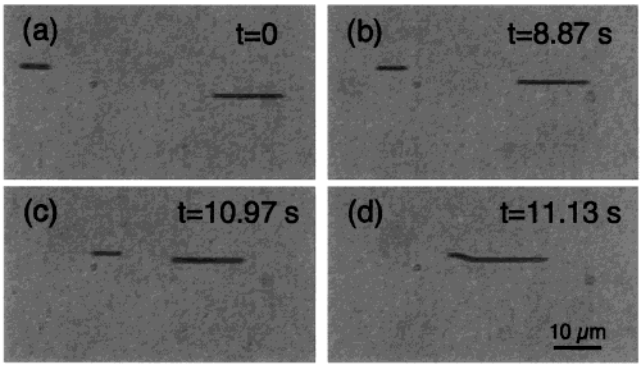

Figure 4. Video microscopy images showing attractive interaction between two Ni nanowires, coaligned in a 1 G external field in a water suspension. The nanowires' lengths are 16.4 and 6.4 μm.

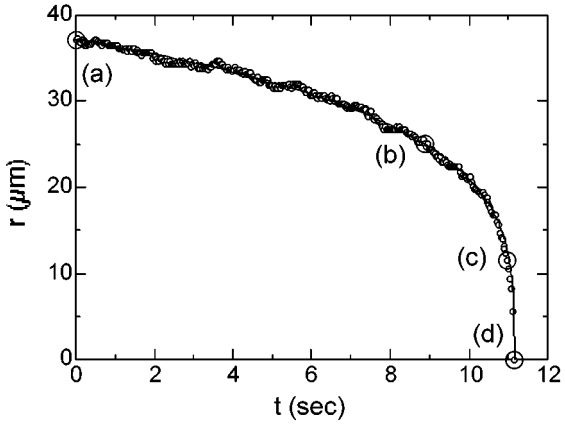

Figure 5. Separation vs time for the pair of nanowires shown in Figure 4. The data points each correspond to a single video frame (point spacing $\Delta t = 1/30$ s). The large circles (a)−(d) indicate the locations of the corresponding images in Figure 4. The solid line is a fit described in the text.

Assembly of the nanowires can be controlled by the application of a small magnetic field $H \sim 1$ G. Since the isolated wires all align parallel to H, their tendency to aggregate in a random way due to the complicated angular dependence of the dipolar forces between randomly oriented wires is prevented, and instead the interwire interactions cause the wires to form head-to-tail chains along the magnetic field lines. As shown in Figure 3, these chains become quite long, and can ultimately extend over hundreds of microns. We have studied the dynamics of this chain formation for wires near the glass bottom of our experimental cells through video microscopy. Videos were taken of a variety of joining events involving either pairs of single nanowires, or pairs of chain segments. Here we present the details of chaining two nanowires, with lengths $L_1 = 16.4 \pm 0.1$ μm and $L_2 = 6.4 \pm 0.1$ μm, suspended in water at temperature $T = 35$ C that come together across an initial separation $r_0 = 37.2$ μm in a time $t_c = 11.1$ s. Four frames from this process are shown in Figure 4. From such data, the position of each wire or chain segment can be determined frame-by-frame using commercial object-tracking software (IgorPro, Wavemetrics, Inc.). The resulting plot of end-to-end separation vs time for the event in Figure 4 is shown in Figure 5. Circles in Figure 5 indicate the data points corresponding to the four frames in Figure 4. All joining events show the basic shape seen here—an initially slow relative motion that speeds up dramatically as the separation closes. The use of higher viscosity solvents such as ethylene glycol results in slower wire motion over comparable distances.

For nanoparticles in fluid suspension, the Reynolds number R is very small ($R < 10^{-5}$ for our nanowires), and hence viscous drag dominates all other hydrodynamic effects.[21,22] Thus, in response to an applied force $\mathbf{F}$, a nanoparticle obtains a velocity $\mathbf{v} = \mathbf{F}/D$, where D is the appropriate drag coefficient. This relationship holds for particles moving under gravitational (settling), electric (electrophoresis), or as in our case, magnetic forces.[23] Nickel nanowires are known to possess a very large remnant magnetization.[24,25] Thus, given their high aspect ratio, for distances large compared to the wire radius a, the magnetic field of a wire is well-approximated by that of an extended dipole with length equal to the wire or chain, and magnetic charges $+Q_m = M\pi a^2$ at one end and $-Q_m$ at the other, where M is the wire's magnetization. For our wires, this approximation is accurate to within 0.05% for distances >5 μm from the wires' ends. The equivalent Coulomb forces between the magnetic charges on the two wires then give the magnetic force between a pair of wires or chain segments. We consider here the special case where the nanowires are aligned collinearly, which is sufficient to analyze the chaining event shown in Figure 4. In this case, the attractive force between two nanowires of lengths L_1 and L_2 is

$$f(r) = -{Q_m}^2\left(\frac{1}{r^2} - \frac{1}{(r+L_1)^2} - \frac{1}{(r+L_1)^2} + \frac{1}{(r+L_1+L_1)^2}\right) \quad (1)$$

where r is the end-to-end wire separation. The time dependence of this separation is determined from the equation of motion $dr/dt = \tilde{D}f(r)$, where $\tilde{D} = D_1D_2/(D_1 + D_2)$ is the reduced drag coefficient. This equation may be integrated analytically to give

$$t(r) = k(F_1(L + r_0, L_1, L_2) = F_1(L + r, L_1, L_2)) \quad (2)$$

Here $L = (L_1 + L_2)/2$, $k = \tilde{D}/m_1m_2$, and $m_{1,2} = M\pi a^2L_{1,2}$ are

the total magnetic moments of the nanowires. The function F_1 is given by

$$F_1(u,L_1,L_2) = \frac{(37{L_1}^4 - 10{L_1}^2{L_2}^2 + 37{L_2}^4)u}{864} - \frac{({L_1}^2 + {L_2}^2)u^3}{108} + \frac{u^5}{30} + \frac{({L_1}^4 - 4{L_1}^2{L_2}^2 + {L_2}^4 - ({L_1}^2 + {L_2}^2)b^2)^2 \operatorname{Arctan}\left(\frac{-i2\sqrt{3}u}{\sqrt{2b^2 + {L_1}^2 + {L_2}^2}}\right)}{i108\sqrt{3}b^2\sqrt{2b^2 + {L_1}^2 + {L_2}^2}} - \frac{({L_1}^4 - 4{L_1}^2{L_2}^2 + {L_2}^4 + ({L_1}^2 + {L_2}^2)b^2)^2 \operatorname{Arctan}\left(\frac{2\sqrt{3}u}{\sqrt{2b^2 + {L_1}^2 + {L_2}^2}}\right)}{108\sqrt{3}b^2\sqrt{2b^2 + {L_1}^2 + {L_2}^2}} \quad (3)$$

with $b = 4\sqrt{{L_1}^4 - 4{L_1}^2{L_2}^2 + {L_2}^4}$. Equation 2 is not readily inverted to give $r(t)$, and therefore we fit our data to $t(r)$. This two-parameter model gives an excellent account of chaining events for a wide variety of wire lengths and initial separations. For the event shown in Figure 4, the model gives the solid line in Figure 5, with $r_0 = 37.2 \pm 0.1$ μm and $k = (1.48 \pm 0.1) \times 10^{-6}$ s/μm^5.

The reduced drag coefficient may be determined from k. Nickel nanowires of this size have been shown to have coercive fields $H_c \sim 200$ G, and remnant magnetizations $M_r \sim 0.7M_{sat}$, where $M_{sat} = 485$ G is the room temperature, bulk saturation magnetization of Ni.[24,25] As these nanowires had been magnetized in fields in excess of 1 kG, with a small bar magnet placed outside the experimental cell, they should possess their full remnant magnetization, i.e., $M = M_r$. On this basis, we obtain $\tilde{D} = 2 \times 10^{-5}$ g/s. We note, however, that there is nearly a 50% uncertainty in this number, arising principally from uncertainty in the nanowires' radius that results from variations in the pore sizes of the alumina templates. In the limit where the nanowires are far from the cell bottom, the drag coefficients D_1 and D_2 for the two nanowires, and hence $\tilde{D}$, can be calculated by approximating the nanowires' shapes as prolate ellipsoids.[22,26] This yields $\tilde{D} = 1.2 \times 10^{-5}$ g/s, in quite good general agreement with our measured value. The determination of $\tilde{D}$ can clearly be refined in the future by using nanowires grown in more uniform templates.

In summary, these studies demonstrate a new magnetic approach for manipulating and orientating nanowires. The dynamics of "chaining" nanowires in fluid solution is quantitatively understood using a theoretical model that assumes viscous drag and magnetic dipole−dipole forces are dominant. This model allows accurate predictions of nanowire dynamics in magnetic fields and an estimate of the reduced drag coefficient. By coating the nanowires with porphyrins, they become highly fluorescent. These nanowires, and many possible variations based upon them, have potential applications in biotechnology and separations chemistry where the powerful optical tracking techniques currently in use can be combined with magnetic manipulation. Studies of the chemical, optical, and magnetic properties of these nanowires in biological media are currently underway in our laboratories.

Acknowledgment. We acknowledge support from the NSF MRSEC Grant DMR00-80031.

References

(1) Musick, M. D.; Pena, D. J.; Botsko, S. L.; McEvoy, T. M.; Richardson, J. N.; Natan, M. J. *Langmuir* **1999**, *15*, 844−850.
(2) Colvin, V. L.; Goldstein, A. N.; Alivisatos, A. P. *J. Am. Chem. Soc.* **1992**, *114*, 5221−5230.
(3) Kagen, C. R.; Murray, C. B.; Nirmal, M.; Bawendi, M. G. *Phys. Rev. Lett.* **1996**, *76*, 1517−1520.
(4) Freeman, R. G.; Graber, K. C.; Allison, K. J.; Bright, R. M.; Davis, J. A.; Guthrie, A. P.; Hommer, M. B.; Jackson, M. A.; Smith, P. C.; Walter, D. G.; Natan, M. G. *Science* **1995**, *267*, 1629−1632.
(5) Whetton, R. L.; Shafigullin, M. N.; Khoury, J. T.; Schaaff, T. G.; Vezmer, I.; Alvarez, M. M.; Wilkinson, A. *Acc. Chem. Res.* **1999**, *32*, 397−406.
(6) Li, H.; Luk, Y. Y.; Mrksich, M. *Langmuir* **1999**, *15*, 4957−4959.
(7) Collier, C. P.; Saykally, R. J.; Shiang, J. J.; Henrichs, S. E.; Heath, J. R. *Science* **1997**, 1978−1981.
(8) Bezryadin, A.; Dekker: C.; Schmid, G. *Appl. Phys. Lett.* **1997**, *71*, 1273−1275.
(9) Sun, S.; Murray, C. B. *J. Appl. Phys.* **1999**, *85*, 4325−4330.
(10) (a) Smith, P. A.; Nordquist, C. D.; Jackson, T. N.; Mayer, T. S.; Martin, B. R.; Mbindyo, J.; Mallouk, T. E. *Appl. Phys. Lett.* **2000**, *77*, 1399−1401. (b) Martin, B. R.; Dermody, D. J.; Reiss, B. D.; Fang, M.; Lyon, A.; Natan, M. J.; Mallouk, T. E. *Adv. Mater.* **1999**, *11*, 1021−1025.
(11) Chang, S.; Shih, C.; Chen, C.; Lai, W.; Wang, C. R. C. *Langmuir* **1999**, *15*, 701−709.
(12) Al-Rawashdeh, N. A. F.; Sandrock, M. L.; Seugling, C. J.; Foss, C. A. *J. Phys. Chem. B* **1998**, *102*, 361−371.
(13) Foss, C. A.; Hornyak, G. L.; Stockhart, J. A.; Martin, C. R. *J. Phys. Chem.* **1994**, *98*, 2963−2971.
(14) Hu, J.; Odom, T. W.; Lieber, C. M. *Acc. Chem. Res.* **1999**, *32*, 435−445.
(15) Korgel, B. A.; Fitzmaurice, D. *Adv. Mater.* **1998**, *10*, 661−665.
(16) Mohamed, M. B.; Volkov, V.; Link, S.; El Sayed, M. *Chem. Phys. Lett.* **2000**, *317*, 517−523.
(17) Whitney, T. M.; Jiang, J. S.; Searson, P. C.; Chien, C. L. *Science* **1993**, *261*, 1316−1319.
(18) Gouterman, M. Optical Spectra and Electronic Structure of Porphyrins and Related Rings. *The Porphyrins, Vol. III*; The Academic Press: New York, 1978.
(19) (a) Kamat, P. V.; Fox, M. A. *Chem. Phys. Lett.* **1983**, *102*, 379−382. (b) Kalyanasundaram, K.; Vlachopoulos, N.; Krishnan, V.; Monnier, A.; Gratzel, M. *J. Phys. Chem.* **1987**, *91*, 2342−2347.
(20) (a) Chance, R.; Prock, A.; Silbey, R. *Adv. Chem Phys.* **1978**, *37*, 1−54. (b) Whitemore, P.; Robota, H.; Harris, C. B. *J. Chem. Phys.* **1982**, *77*, 1560−1565.
(21) Landau, L.; Lifshitz, E. *Fluid Mechanics*; Pergamon: London, 1959.
(22) The nanowires proximity to the cell bottom may modify hydrodynamics, and this is not included in our modeling. However, the agreement between predicted and observed behavior strongly suggests that the relatively simple model described is sufficient for the chaining events studied.
(23) Hunter, R. J. *Introduction to Modern Colloid Science*; Oxford: New York, 1993.
(24) Fert, A.; Piraux, L. *J. Magn. Magn. Mater.* **1999**, *200*, 338−358.
(25) Sun, L.; Searson, P. C.; Chien, C. L. *Appl. Phys. Lett.* **1999**, *74*, 2803−2805.
(26) Lamb, H. *Hydrodynamics*, 6th ed.; Dover: New York, 1945.

NL005532S